

THE CN-CH POSITIVE CORRELATION IN THE GLOBULAR CLUSTER NGC 5286

DONGWOOK LIM, SEUNGSOO HONG, AND YOUNG-WOOK LEE

Center for Galaxy Evolution Research & Department of Astronomy, Yonsei University, Seoul 03722, Korea;
dwlim@yonsei.ac.kr, ywlee2@yonsei.ac.kr

ABSTRACT

We performed low-resolution spectroscopy for the red giant stars in the Galactic globular cluster (GC) NGC 5286, which is known to show intrinsic heavy element abundance variations. We found that the observed stars in this GC are clearly divided into three subpopulations by CN index (CN-weak, CN-intermediate, and CN-strong). The CN-strong stars are also enhanced in the calcium HK' (7.4σ) and CH (5.1σ) indices, while the CN-intermediate stars show no significant difference in the strength of HK' index with CN-weak stars. From the comparison with high-resolution spectroscopic data, we found that the CN- and HK'-strong stars are also enhanced in the abundances of Fe and *s*-process elements. It appears, therefore, that these stars are later generation stars affected by some supernovae enrichment in addition to the asymptotic giant branch ejecta. In addition, unlike normal GCs, sample stars in NGC 5286 show the CN-CH positive correlation, strengthening our previous suggestion that this positive correlation is only discovered in GCs with heavy element abundance variations such as M22 and NGC 6273.

Keywords: globular clusters: general — globular clusters: individual (NGC 5286) — stars: abundances — stars: evolution — techniques: spectroscopic

1. INTRODUCTION

During the last two decades, an increasing number of observations have shown that most of the Milky Way globular clusters (GCs) host multiple stellar populations, each of which has different chemical properties (e.g., Lee et al. 1999; Carretta et al. 2009; Gratton et al. 2012; Piotto et al. 2015, and references therein). These GCs share similar characteristics, such as light element abundance variations and a central concentration of later generation stars (e.g., Carretta et al. 2009; Lardo et al. 2011), although some exceptional cases are also reported. The abundance variations in the light elements, discovered in most GCs, are explained as an enrichment and/or pollution by intermediate-mass asymptotic giant branch (AGB) stars (D'Antona & Caloi 2004; D'Antona et al. 2016), massive interacting binary stars (de Mink et al. 2009; Bastian et al. 2013), and fast-rotating massive stars (FRMSs; Prantzos & Charbonnel 2006; Decressin et al. 2007). Several GCs with heavy element abundance variations, including ω -Centauri and M22 (Lee et al. 1999; J.-W. Lee et al. 2009; Marino et al. 2009; Johnson & Pilachowski 2010), however, show evidence of supernovae (SNe) enrichment, which suggests that they were massive enough in the past to retain SNe ejecta (Baumgardt et al. 2008; Šilich & Tenorio-Tagle 2017). In the hierarchical merging paradigm, they would have contributed to the formation of the Milky Way, since these GCs could be former nuclei of dwarf galaxies (see Lee et al. 2007; Han et al. 2015; Da Costa 2016), and therefore, would help to solve the “missing satellites prob-

lem” (Klypin et al. 1999; Moore et al. 1999, 2006).

A direct way to find these unique GCs is a measurement of heavy element abundance of stars in a GC using high-resolution spectroscopy (e.g., Da Costa et al. 2009; Yong et al. 2014; Johnson et al. 2015). However, our previous studies have demonstrated that the low-resolution spectroscopy for the calcium HK' index can be used to more effectively detect the heavy element variations in a GC (Lim et al. 2015; Han et al. 2015). Interestingly, we found that these GCs also show the CN-CH positive correlation among red giant branch (RGB) stars, unlike the CN-CH anticorrelation generally observed in “normal” GCs (Suntzeff & Smith 1991; S.-G. Lee 2005; Kayser et al. 2008; Pancino et al. 2010; Smolinski et al. 2011). If confirmed, this would imply that the CN-CH positive correlation can be used as a probe for the GCs with heavy element variations.

In order to further confirm our conjecture, we have performed low-resolution spectroscopy for the RGB stars in NGC 5286. This GC is relatively poorly studied, although Marino et al. (2015, hereafter M15) recently showed some abundance variations in Fe and *s*-process elements among RGB stars from high-resolution spectroscopy. The purpose of this paper is to report that RGB stars in this GC are clearly divided into three subpopulations by CN index, and CN-strong stars are also enhanced in the calcium HK' and CH indices, indicating the CN-CH positive correlation.

2. OBSERVATIONS AND DATA REDUCTION

Our observations were performed with the du Pont 2.5m telescope at Las Campanas Observatory (LCO) during four nights from April to June 2016. We have used multi-object spectroscopy mode of Wide Field Reimaging CCD Camera (WFCCD) with HK grism, which provides a dispersion of $0.8 \text{ \AA}/\text{pixel}$ and a central wavelength of 3700 \AA . Spectroscopic target stars are selected from the 2MASS All-Sky Point Source Catalog. In particular, we have included a number of stars observed by M15 for the comparison with high-resolution spectroscopy. For these observations, three multi-slit masks, each of which contains about 25 slits of $1''.2$ width, were designed. We had obtained four 1500-second science exposures, three flats, and an arc lamp frame for each mask. The data reduction was performed with IRAF¹ and the modified version of the WFCCD reduction package, following Lim et al. (2015) and Prochaska et al. (2006). The radial velocity (RV) of each star was measured using *rvidlines* task in the IRAF RV package, and the signal-to-noise ratio (S/N) was estimated at $\sim 3900 \text{ \AA}$. After the rejection of non-member stars ($RV > 2.0\sigma$ of the mean velocity of the GC) and low S/N (< 8.0) spectra, 44 stars are finally used for our analysis. The median RV for these stars is 52.5 km/s , which is comparable to but somewhat smaller than the value of 57.4 km/s reported by Harris (2010) and 61.5 km/s estimated by M15. Compared to the RVs measured from high-resolution spectroscopy, the typical uncertainty of those from our low-resolution measurement appears to be quite large ($\sim 20 \text{ km/s}$). Figure 1 shows the selected sample stars on the color-magnitude diagram (CMD), for which the photometry was obtained at the LCO 2.5m du Pont telescope. Fifteen target stars, however, are outside the field-of-view (FOV) of the photometry ($8'.85 \times 8'.85$) and therefore not plotted in this CMD. A detailed description of this photometry can be found in Lim et al. (2015).

Finally, we measured the S(3839) index for CN band, the HK' index for Ca II H and K lines, and the CH4300 index for CH band of each target star in NGC 5286, following Lim et al. (2015). The definitions for these indices are

$$\begin{aligned} \text{HK}' &= -2.5 \log \frac{F_{3916-3985}}{2F_{3894-3911} + F_{3990-4025}}, \\ \text{CN}(3839) &= -2.5 \log \frac{F_{3861-3884}}{F_{3894-3910}}, \\ \text{CH4300} &= -2.5 \log \frac{F_{4285-4315}}{0.5F_{4240-4280} + 0.5F_{4390-4460}}, \end{aligned}$$

where $F_{3916-3985}$, for example, is the integrated flux from 3916 to 3985 \AA . All of these indices are defined as the ratio of the absorption strength to nearby continuum strength. The measurement error for each sample was estimated from

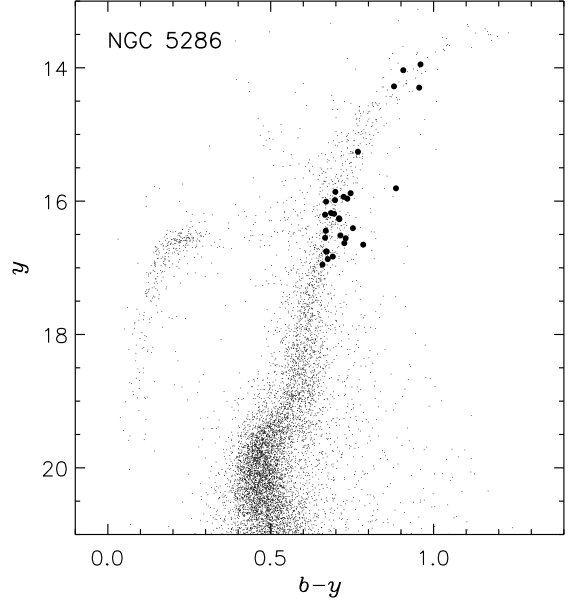


Figure 1. Our CMD for NGC 5286 in the $(y, b-y)$ plane obtained at the LCO 2.5m du Pont telescope. Black circles indicate selected sample stars in the spectroscopic analysis. Note that some target stars are outside the FOV of the photometry and therefore not plotted in this CMD.

Poisson statistics in the flux measurements (Vollmann & Eversberg 2006). In addition, we measured the delta indices (δCN , $\delta\text{HK}'$, and δCH) to compare the chemical abundances of stars without the effect of magnitude in the same manner as in previous studies (e.g., Norris et al. 1981; Harbeck et al. 2003). These δ -indices are calculated as the difference between the original index for each star and the least-squares fitting of the full sample (black solid lines in the left panels of Figure 2) in a GC. The measured indices and errors are listed in Table 1.

3. MULTIPLE STELLAR POPULATIONS IN NGC 5286

Figure 2 shows the measured spectral indices of stars as functions of K magnitude, obtained from 2MASS catalog. The CN, HK', and CH indices increase with decreasing magnitude because the brighter RGB stars have lower temperatures and the strengths of these molecular bands generally increase with decreasing temperature. Therefore the chemical abundances of stars are compared on the δ -index versus magnitude diagrams. It is important to note that the observed stars show a large spread in δ -index that is at least several times larger than the measurement error. The standard deviations for all sample stars are 0.23 for CN, 0.07 for HK', and 0.07 for CH. In particular, the CN index distribution shows the largest spread. Note that a bimodality or a large spread in CN distribution is generally observed in most GCs (Norris et al. 1981; Norris 1987; Briley et al. 1992; Har-

¹ IRAF is distributed by the National Optical Astronomy Observatory, which is operated by the Association of Universities for Research in Astronomy (AURA) under a cooperative agreement with the National Science Foundation.

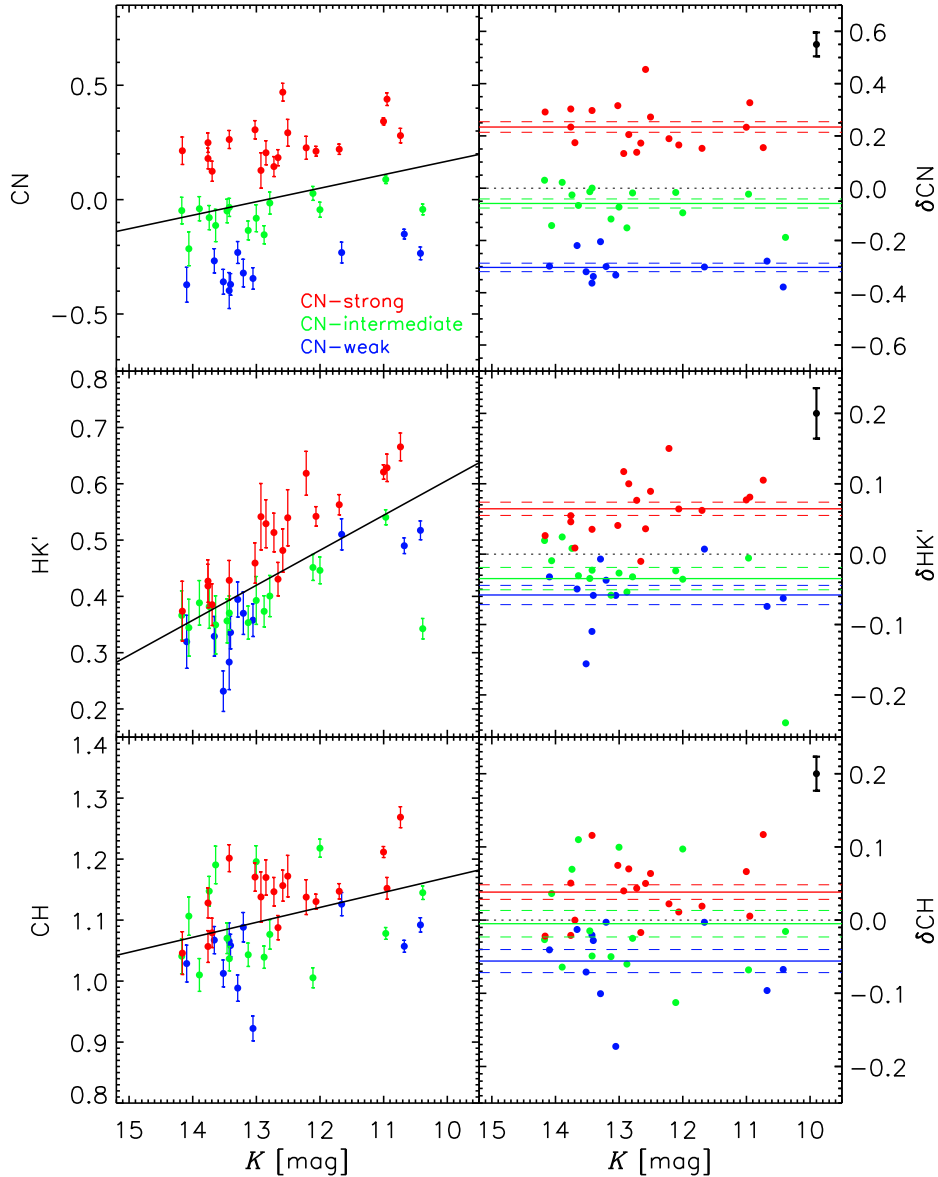


Figure 2. Left panels: measured spectral indices (CN, HK' and CH) as functions of K magnitude for RGB stars in NGC 5286, where the blue, green, and red circles are CN-weak, CN-intermediate, and CN-strong stars. Right panels: the δ CN, δ HK', and δ CH indices plotted against K magnitude. The CN-strong stars are enhanced not only in CN index but also in HK' and CH indices. We note that CN-weak and CN-intermediate subpopulations show similar strengths of the HK' index, whereas they are clearly separated in the CN index. The mean value and the error of the mean ($\pm 1\sigma$) for each subpopulation are denoted by solid and dashed lines, respectively. The vertical bars in the upper right corner indicate the typical measurement error for each index.

beck et al. 2003; Kayser et al. 2008; Martell et al. 2008)². Therefore, we have divided subpopulations of RGB stars in NGC 5286 on the histogram of the δ CN index (see Figure 3). It is clear from this histogram that RGB stars are divided into three subpopulations: CN-weak (δ CN < -0.2 ; blue circles), CN-intermediate ($-0.2 \leq \delta$ CN < 0.1 ; green circles), and CN-strong ($0.1 \leq \delta$ CN; red circles). The distribution of CN index

into three or more subpopulations is similar to that reported in NGC 1851 (Campbell et al. 2012; Lim et al. 2015; Simpson et al. 2017). This is also consistent with the recent results from population models and spectroscopic observations which show that most GCs host three or more subpopulations (see, e.g., Jang et al. 2014; Carretta 2015). The presence of multiple populations is also observed from recent photometry using UV filters, which are mainly sensitive to N abundance (Milone et al. 2015; Piotto et al. 2015). In this regard, further observations are required to see that the trimodal CN distribution, observed in NGC 1851 and NGC 5286, is a ubiquitous feature in other GCs as well.

² Although the evolutionary mixing effect can also contribute to the large spread in CN index distribution among bright RGB stars (Sweigart & Mengel 1979), this effect alone cannot explain a discrete distribution and a wide spread in the unevolved stars (see, e.g., Kayser et al. 2008).

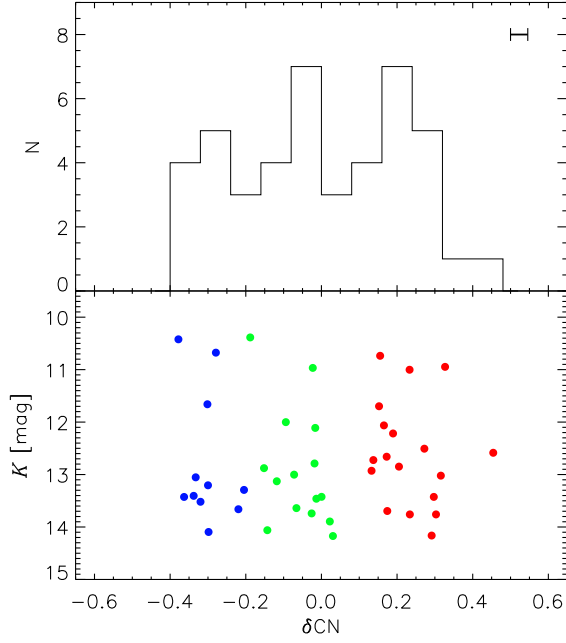


Figure 3. Histogram and distribution of the δCN index for the sample stars. We note that the presence of three subpopulations – CN-weak (blue), CN-intermediate (green), and CN-strong (red) – is shown. The horizontal bar in the upper panel denotes the typical measurement error.

As shown in the right panels of Figure 2, the CN-strong subpopulation is significantly enhanced also in the $\delta\text{HK}'$ and δCH indices. The differences between CN-strong and CN-weak subpopulations are 0.537 for δCN , 0.123 for $\delta\text{HK}'$, and 0.094 for δCH , which are significant at the levels of 20.7σ , 7.4σ , and 5.1σ , respectively, compared to the standard deviation of the mean. The CN-intermediate stars, however, show no clear difference in the strength of $\delta\text{HK}'$ index with CN-weak stars ($\Delta\delta\text{HK}' = 0.02$). Therefore, three subpopulations in the NGC 5286 can be characterized as CN-weak/HK'-weak, CN-intermediate/HK'-weak, and CN-strong/HK'-strong. In particular, the difference in calcium abundance (HK') suggests that this GC also belongs to the group of unique GCs showing intrinsic dispersion in heavy element abundance, in agreement with a result by M15 based on Fe and s -process elements³. The fact that CN-strong stars are also enhanced in the CH band implies a presence of CN-CH positive correlation in this GC (see Section 4 below).

In order to see whether the CN- and HK'-strong stars in our study are also enhanced in Fe and s -process elements, we have compared our results with high-resolution spectroscopy by M15. In Figure 4, our δCN and $\delta\text{HK}'$ indices are plot-

³ Mucciarelli et al. (2015) questioned the presence of an intrinsic Fe spread in some GCs, including M22. They found no obvious Fe spread when Fe abundance is measured from Fe II line with photometric gravity. On the other hand, J.-W. Lee (2016) has refuted this claim from the independent spectroscopic analysis. In any case, the presence of apparent Ca spread in these GCs would suggest that they were affected by SNe enrichment.

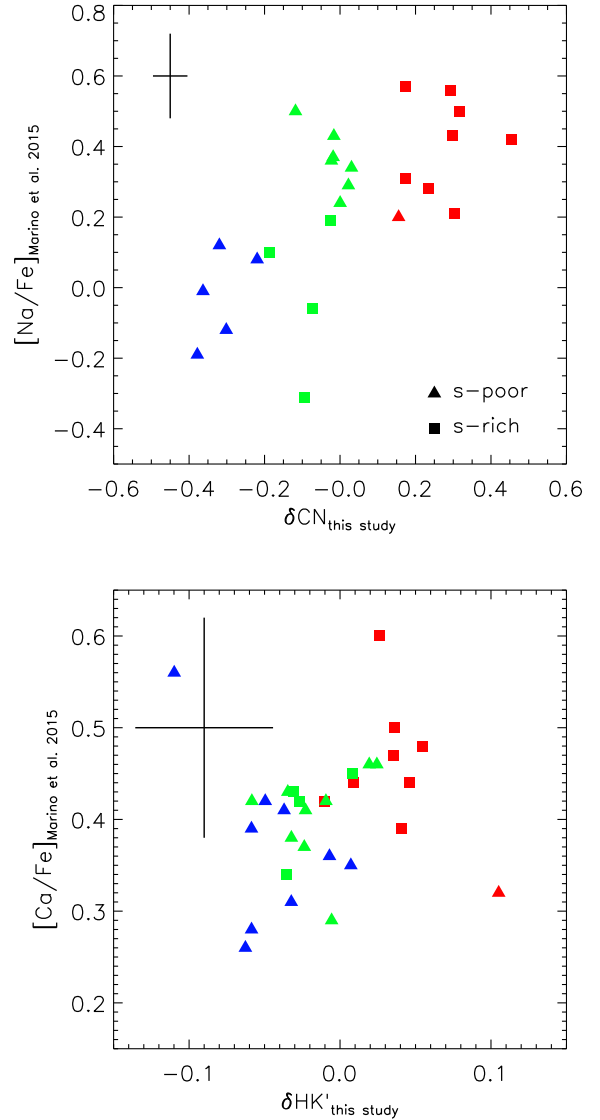


Figure 4. Comparison between our study and high-resolution spectroscopy by M15. The $[\text{Na}/\text{Fe}]$ and $[\text{Ca}/\text{Fe}]$ abundances measured by M15 are plotted against the δCN and $\delta\text{HK}'$ indices of this study, respectively. The blue, green, and red colors indicate the CN-weak, CN-intermediate, and CN-strong stars, divided in this study, and triangles and squares are s -poor and s -rich stars, identified by M15. The typical measurement error is plotted on the upper-left corner. Note that both diagrams show good correlations with a few exceptions. In addition, our subgrouping by CN index is similar to that by s -process elements.

ted with $[\text{Na}/\text{Fe}]$ and $[\text{Ca}/\text{Fe}]$ abundances, respectively, for 33 common stars. In general, the strength of CN band is correlated with the N and Na abundances, while the CH band is affected by C abundance (Snedden et al. 1992; Smith et al. 1996; Marino et al. 2008). The upper panel of Figure 4 also shows a strong correlation between $[\text{Na}/\text{Fe}]$ and δCN index, which is in good agreement with previous studies (Snedden et al. 1992; Lim et al. 2016)⁴. The CN-weak (blue) and

⁴ Careful inspection of the upper panel of Figure 4 also shows the possibility that the s -poor and s -rich groups are probably separated on this diagram,

CN-strong (red) subpopulations are almost identical to the s -poor (triangles) and s -rich (squares) groups, respectively. In addition, the $\delta\text{HK}'$ index is understandably correlated with the $[\text{Ca}/\text{Fe}]$ abundance with a few exceptions (see the lower panel of Figure 4). According to this comparison, the difference in $\delta\text{HK}'$ index between CN-weak and CN-strong stars (~ 0.094) is equivalent to 0.09 dex in $\Delta[\text{Ca}/\text{Fe}]$ and 0.15 dex in $\Delta[\text{Fe}/\text{H}]$. These comparisons confirm that our results from low-resolution spectroscopy are consistent with those from high-resolution spectroscopy by M15. Consequently, the later generation stars in NGC 5286 show the enhancements not only in light elements (CN) but also in heavy elements (Fe and Ca) and s -process elements, although the presence of Fe spread requires further investigations (see Mucciarelli et al. 2015; J.-W. Lee 2016).

4. THE CN-CH POSITIVE CORRELATION IN GLOBULAR CLUSTERS WITH HEAVY ELEMENT VARIATIONS

As described above, the CN-CH anticorrelation is one of the typical features in the low-resolution spectroscopic studies of GCs (Suntzeff & Smith 1991; Kraft 1994; Harbeck et al. 2003; S.-G. Lee 2005; Pancino et al. 2010; Smolinski et al. 2011, and references therein). This feature is most likely due to the anticorrelation between C and N abundances (see, e.g., Smith et al. 1996; Cohen et al. 2005). In the multiple population paradigm, the mechanism responsible for the Na-O anticorrelation would also produce C-N anticorrelation (Ventura et al. 2013; Di Criscienzo et al. 2016). Our previous studies, however, found a significant CN-CH positive correlation, instead of an anticorrelation, among RGB stars in M22 and NGC 6273 (Han et al. 2015; Lim et al. 2015). Interestingly, both GCs are known to host multiple stellar populations with different heavy element abundances (see also Marino et al. 2011; Johnson et al. 2017). Since NGC 5286 is also one of the GCs showing spreads in the abundances of heavy elements, we would expect a similar positive correlation between CN and CH indices. As expected, Figure 5 shows that δCN and δCH indices are positively correlated similarly to the cases of M22 and NGC 6273.

In order to establish how the heavy element abundance variations would affect the CN-CH relation of GCs, we have plotted in Figure 6 the δCN versus δCH diagrams for six GCs (NGC 288, NGC 6723, NGC 1851, NGC 6273, M22, and NGC 5286), together with the $\delta\text{HK}'$ distributions. The spectroscopic and photometric data are taken from Han et al. (2015) and Lim et al. (2015, 2016). The slope of the CN-CH

with the s -rich stars more enhanced in both $[\text{Na}/\text{Fe}]$ and δCN . This would imply that the variations in light elements would be present in each group with different s -process elements abundances, which has already been found in other GCs with s -process element and Fe variations, such as M2 and M22 (Marino et al. 2011; Yong et al. 2014). More sample of stars, however, are needed to confirm this trend in NGC 5286.

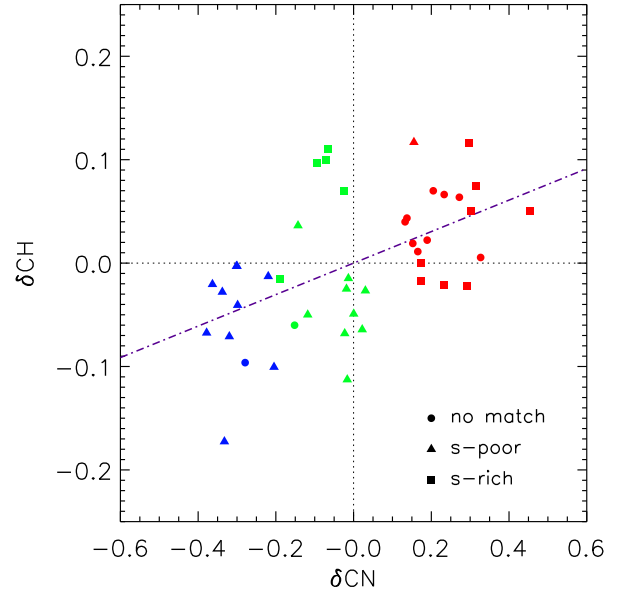


Figure 5. Correlation between δCN and δCH indices of our sample stars in NGC 5286. They show a positive correlation similarly to the cases of M22 and NGC 6273. Symbols are same as in Figure 4, but circles represent stars only observed in our study. The purple line indicates a least-square fit.

relation for each GC is estimated by maximum likelihood, and the values are listed in the upper panels of Figure 6. We can see from this figure that normal GCs without a difference in Ca abundance, NGC 288 and NGC 6723, show the conventional CN-CH anticorrelation. On the contrary, GCs with the difference in HK' index between the two subpopulations, NGC 6273, M22, and NGC 5286, show the CN-CH positive correlation. In the case of NGC 1851, the difference in HK' index is relatively small, and the CN-CH relation seems to be flat⁵. In order to test the significance of the correlation, we have calculated the Spearman's rank correlation coefficient for each GC. The obtained correlation coefficient are -0.52 and -0.62 for NGC 288 and NGC 6723, -0.05 for NGC 1851, and +0.37, +0.61, and +0.52 for NGC 6273, M22, and NGC 5286, respectively. The p -values are very small (7.3×10^{-7} , 1.4×10^{-4} , 7.3×10^{-4} , 2.9×10^{-11} , and 2.9×10^{-4} for NGC 288, NGC 6723, NGC 6273, M22, and NGC 5286), confirming that the correlations are statistically significant, except for NGC 1851 (p -value = 0.72). Because the negative Spearman coefficient (-1.0 \sim 0.0) indicates anticorrelation while the positive coefficient (0.0 \sim +1.0) is for positive correlation, this result confirms the systematic variation in the CN-CH correlation among sample GCs. Therefore, the origin of the CN-CH positive correlation appears to be explicitly relevant to the heavy element abundance variations. In this respect, it would be interesting to measure

⁵ Recently, Simpson et al. (2017) discovered seven stars strongly enhanced in both CN and CH indices in NGC 1851.

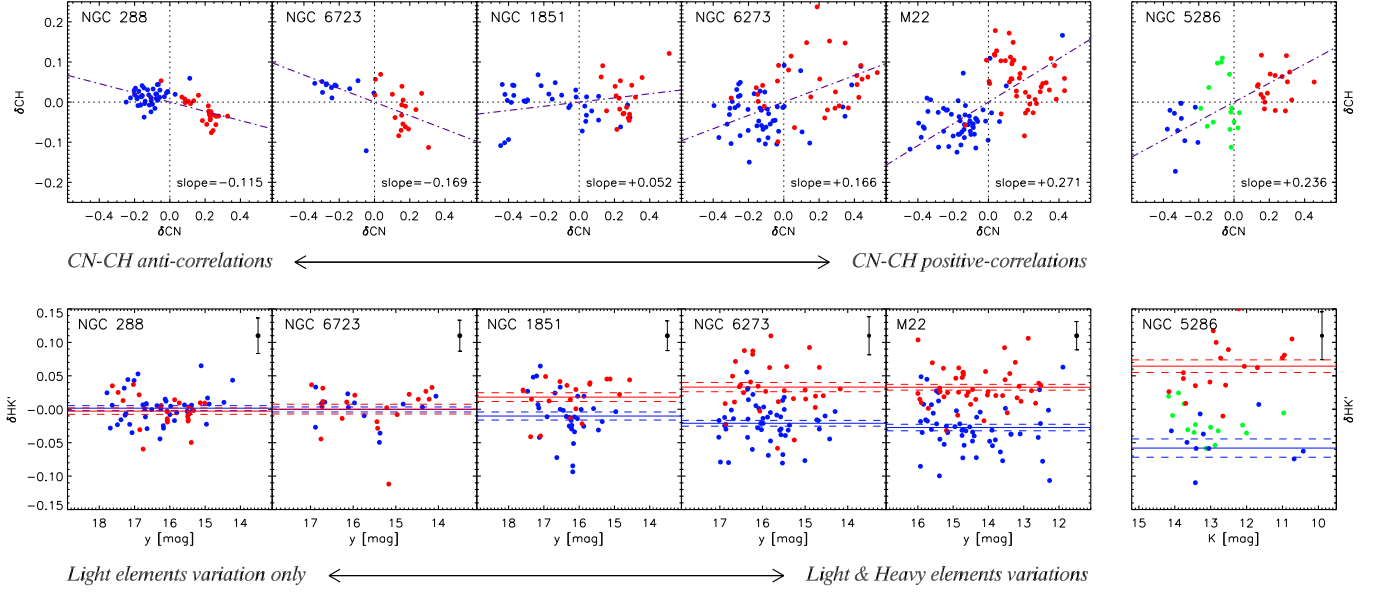


Figure 6. The CN-CH correlations and the $\delta\text{HK}'$ index distributions for six GCs (NGC 288, NGC 6723, NGC 1851, NGC 6273, M22, and NGC 5286). Colors and symbols are same as in Figures 2 and 5. The GCs with the difference in Ca abundances (HK') show the CN-CH positive correlation, while the normal GCs show the general CN-CH anticorrelation. NGC 5286 also shows the CN-CH positive correlation with the difference in HK' index, following the same trend. In the case of NGC 1851, the CN-CH relation seems to be flat (see text).

[C/Fe], [N/Fe], and the C+N+O sum from high-resolution spectroscopy.

As discussed in Lim et al. (2015), the origin of the CN-CH positive correlation, as well as of the heavy element abundance variations, is most likely because the later generation stars are enriched by some SNe in addition to the intermediate-mass AGB stars and/or FRMSs. Unlike the intermediate-mass AGB stars, which are suggested to be mainly responsible for the N-enhancement and C-depletion of later generation stars, the SNe ejecta would supply both N and C elements together with other heavy elements. Our result for the CN-CH positive correlation in NGC 5286 (Figure 5) appears to be similar to those of M22 and NGC 6273. Interestingly, inspection of Figure 2 shows that the observed stars in NGC 5286 can be divided into three subpopulations: CN-weak/ HK' -weak stars (first generation; G1), CN-intermediate/ HK' -weak stars (second generation; G2), and CN-strong/ HK' -strong stars (third generation; G3). These differences in chemical properties imply that the SNe enrichment played a role only in the formation of G3 stars, whereas it had almost no impact on the formation of G2

stars. Although the origin of this complex chemical enrichment requires further investigation, one possibility is a time-dependent gas removal of SNe ejecta in a proto-GC. For example, a recent hydrodynamical simulation by Caproni et al. (2017) shows that the gas removal in a dwarf galaxy was more efficient in the first 600 Myr, while most of the gas could be retained later when the type II SNe rate was significantly decreased. Similar to this, the SNe ejecta could have fully escaped from the proto-NGC 5286 in the early phase, while some of them could have been retained later with decreasing SNe rate. This would explain the absence and presence of some SNe enrichment in G2 and G3, respectively.

We are grateful to the anonymous referee for a number of helpful suggestions. We also thank Sang-II Han for providing photometric data for Figure 1. Support for this work was provided by the National Research Foundation of Korea to the Center for Galaxy Evolution Research, and through the grant programs No. 2017R1A6A3A11031025 and No. 2017R1A2B3002919.

REFERENCES

- Bastian, N., Lamers, H. J. G. L. M., de Mink, S. E., et al. 2013, MNRAS, 436, 2398
- Baumgardt, H., Kroupa, P., & Parmentier, G. 2008, MNRAS, 384, 1231
- Briley, M. M., Smith, G. H., Bell, R. A., Oke, J. B., & Hesser, J. E. 1992, ApJ, 387, 612
- Campbell, S. W., Yong, D., Wylie-de Boer, E. C., et al. 2012, ApJL, 761, L2
- Caproni, A., Amaral Lanfranchi, G., Campos Baio, G. H., Kowal, G., & Falceta-Gonçalves, D. 2017, ApJ, 838, 99
- Carretta, E. 2015, ApJ, 810, 148
- Carretta, E., Bragaglia, A., Gratton, R. G., et al. 2009, A&A, 505, 117
- Cohen, J. G., Briley, M. M., & Stetson, P. B. 2005, AJ, 130, 1177
- Da Costa, G. S. 2016, The General Assembly of Galaxy Halos: Structure, Origin and Evolution, 317, 110
- Da Costa, G. S., Held, E. V., Saviane, I., & Gullieuszik, M. 2009, ApJ, 705, 1481
- D'Antona, F., & Caloi, V. 2004, ApJ, 611, 871

- D'Antona, F., Vesperini, E., D'Ercole, A., et al. 2016, *MNRAS*, 458, 2122
- Decressin, T., Meynet, G., Charbonnel, C., Prantzos, N., & Ekström, S. 2007, *A&A*, 464, 1029
- de Mink, S. E., Pols, O. R., Langer, N., & Izzard, R. G. 2009, *A&A*, 507, L1
- Di Criscienzo, M., Ventura, P., García-Hernández, D. A., et al. 2016, *MNRAS*, 462, 395
- Gratton, R. G., Carretta, E., & Bragaglia, A. 2012, *A&A Rv*, 20, 50
- Han, S.-I., Lim, D., Seo, H., & Lee, Y.-W. 2015, *ApJL*, 813, L43
- Harbeck, D., Smith, G. H., & Grebel, E. K. 2003, *AJ*, 125, 197
- Harris, W. E. 2010, arXiv:1012.3224
- Jang, S., Lee, Y.-W., Joo, S.-J., & Na, C. 2014, *MNRAS*, 443, L15
- Johnson, C. I., Caldwell, N., Rich, R. M., et al. 2017, *ApJ*, 836, 168
- Johnson, C. I., & Pilachowski, C. A. 2010, *ApJ*, 722, 1373
- Johnson, C. I., Rich, R. M., Pilachowski, C. A., et al. 2015, *AJ*, 150, 63
- Kayser, A., Hilker, M., Grebel, E. K., & Willemsen, P. G. 2008, *A&A*, 486, 437
- Klypin, A., Kravtsov, A. V., Valenzuela, O., & Prada, F. 1999, *ApJ*, 522, 82
- Kraft, R. P. 1994, *PASP*, 106, 553
- Lardo, C., Bellazzini, M., Pancino, E., et al. 2011, *A&A*, 525, A114
- Lee, J.-W. 2016, *ApJS*, 226, 16
- Lee, J.-W., Kang, Y.-W., Lee, J., & Lee, Y.-W. 2009, *Nature*, 462, 480
- Lee, S.-G. 2005, *Journal of Korean Astronomical Society*, 38, 23
- Lee, Y.-W., Gim, H. B., & Casetti-Dinescu, D. I. 2007, *ApJL*, 661, L49
- Lee, Y.-W., Joo, J.-M., Sohn, Y.-J., et al. 1999, *Nature*, 402, 55
- Lim, D., Han, S.-I., Lee, Y.-W., et al. 2015, *ApJS*, 216, 19
- Lim, D., Lee, Y.-W., Pasquato, M., Han, S.-I., & Roh, D.-G. 2016, *ApJ*, 832, 99
- Marino, A. F., Milone, A. P., Karakas, A. I., et al. 2015, *MNRAS*, 450, 815 (M15)
- Marino, A. F., Milone, A. P., Piotto, G., et al. 2009, *A&A*, 505, 1099
- Marino, A. F., Sneden, C., Kraft, R. P., et al. 2011, *A&A*, 532, A8
- Marino, A. F., Villanova, S., Piotto, G., et al. 2008, *A&A*, 490, 625
- Martell, S. L., Smith, G. H., & Briley, M. M. 2008, *PASP*, 120, 7
- Milone, A. P., Marino, A. F., Piotto, G., et al. 2015, *ApJ*, 808, 51
- Moore, B., Diemand, J., Madau, P., Zemp, M., & Stadel, J. 2006, *MNRAS*, 368, 563
- Moore, B., Ghigna, S., Governato, F., et al. 1999, *ApJL*, 524, L19
- Mucciarelli, A., Lapenna, E., Massari, D., et al. 2015, *ApJ*, 809, 128
- Norris, J. 1987, *ApJL*, 313, L65
- Norris, J., Cottrell, P. L., Freeman, K. C., & Da Costa, G. S. 1981, *ApJ*, 244, 205
- Pancino, E., Rejkuba, M., Zoccali, M., & Carrera, R. 2010, *A&A*, 524, A44
- Piotto, G., Milone, A. P., Bedin, L. R., et al. 2015, *AJ*, 149, 91
- Prantzos, N., & Charbonnel, C. 2006, *A&A*, 458, 135
- Prochaska, J. X., Weiner, B. J., Chen, H.-W., & Mulchaey, J. S. 2006, *ApJ*, 643, 680
- Silich, S., & Tenorio-Tagle, G. 2017, *MNRAS*, 465, 1375
- Simpson, J. D., Martell, S. L., & Navin, C. A. 2017, *MNRAS*, 465, 1123
- Smith, G. H., Shetrone, M. D., Bell, R. A., Churchill, C. W., & Briley, M. M. 1996, *AJ*, 112, 1511
- Smolinski, J. P., Martell, S. L., Beers, T. C., & Lee, Y. S. 2011, *AJ*, 142, 126
- Sneden, C., Kraft, R. P., Prosser, C. F., & Langer, G. E. 1992, *AJ*, 104, 2121
- Suntzeff, N. B., & Smith, V. V. 1991, *ApJ*, 381, 160
- Sweigart, A. V., & Mengel, J. G. 1979, *ApJ*, 229, 624
- Ventura, P., Di Criscienzo, M., Carini, R., & D'Antona, F. 2013, *MNRAS*, 431, 3642
- Vollmann, K., & Eversberg, T. 2006, *Astronomische Nachrichten*, 327, 862
- Yong, D., Roederer, I. U., Grundahl, F., et al. 2014, *MNRAS*, 441, 3396

Table 1. Index Measurements for the sample stars in NGC 5286

ID	R.A.	Decl.	K	CN	errCN	δ CN	HK'	errHK'	δ HK'	CH	errCH	δ CH	ID _{M15}
N5286-1001	206.39160	-51.45328	11.6980	0.2202	0.0225	0.1524	0.5628	0.0180	0.0622	1.1472	0.0126	0.0190	–
N5286-1004	206.42943	-51.41643	11.0020	0.3421	0.0153	0.2331	0.6209	0.0128	0.0770	1.2116	0.0090	0.0663	–
N5286-1005	206.36223	-51.34178	12.5070	0.2922	0.0586	0.2722	0.5396	0.0499	0.0892	1.1720	0.0340	0.0637	–
N5286-1006	206.36823	-51.34811	12.2170	0.2265	0.0503	0.1894	0.6185	0.0390	0.1502	1.1377	0.0285	0.0222	–
N5286-1007	206.36032	-51.39484	12.0630	0.2115	0.0215	0.1653	0.5421	0.0173	0.0642	1.1304	0.0121	0.0111	–
N5286-1008	206.48909	-51.42993	10.6760	-0.1508	0.0214	-0.2790	0.4899	0.0139	-0.0743	1.0571	0.0098	-0.0962	–
N5286-1045	206.74561	-51.36780	12.8490	0.2049	0.0527	0.2050	0.5290	0.0426	0.1000	1.1699	0.0289	0.0699	–
N5286-1046	206.74057	-51.37590	12.8780	-0.1537	0.0395	-0.1518	0.3734	0.0276	-0.0539	1.0392	0.0183	-0.0601	–
N5286-1067	206.79630	-51.30748	12.9280	0.1277	0.0775	0.1326	0.5415	0.0590	0.1173	1.1379	0.0411	0.0399	–
N5286-1068	206.78522	-51.40542	12.7240	0.1445	0.0438	0.1373	0.5134	0.0344	0.0765	1.1465	0.0234	0.0435	–
N5286-1077	206.39413	-51.31052	10.9470	0.4391	0.0276	0.3269	0.6283	0.0244	0.0810	1.1521	0.0178	0.0054	–
N5286-3002	206.58405	-51.35508	10.7360	0.2799	0.0316	0.1552	0.6655	0.0246	0.1051	1.2687	0.0172	0.1169	527G
N5286-3004	206.60188	-51.36125	10.3860	-0.0429	0.0236	-0.1882	0.3426	0.0182	-0.2396	1.1449	0.0111	-0.0155	757G
N5286-3005	206.59503	-51.32511	13.5190	-0.3595	0.0544	-0.3197	0.2316	0.0360	-0.1559	1.0126	0.0221	-0.0710	697G
N5286-3007	206.57454	-51.34800	13.0210	0.3054	0.0401	0.3157	0.4591	0.0358	0.0407	1.1705	0.0232	0.0748	399G
N5286-3009	206.63637	-51.34433	10.4220	-0.2349	0.0278	-0.3781	0.5173	0.0167	-0.0627	1.0921	0.0118	-0.0674	1297G
N5286-3010	206.71512	-51.35806	13.8950	-0.0398	0.0529	0.0222	0.3885	0.0396	0.0244	1.0101	0.0269	-0.0642	1767G
N5286-3011	206.63579	-51.32022	13.6950	0.1239	0.0440	0.1741	0.3852	0.0370	0.0087	1.0791	0.0241	-0.0001	1269G
N5286-3012	206.61157	-51.33022	13.7600	0.1798	0.0452	0.2338	0.4184	0.0386	0.0459	1.0567	0.0261	-0.0209	939G
N5286-3014	206.61841	-51.31781	13.2930	-0.2311	0.0479	-0.2047	0.3945	0.0312	-0.0070	0.9885	0.0216	-0.1005	1057G
N5286-3015	206.65620	-51.33216	13.2050	-0.3211	0.0605	-0.2999	0.3699	0.0375	-0.0371	1.0883	0.0241	-0.0029	1547G
N5286-3017	206.71629	-51.38522	13.0530	-0.3447	0.0471	-0.3324	0.3577	0.0290	-0.0587	0.9224	0.0204	-0.1726	5441G
N5286-3020	206.68457	-51.34958	13.4260	0.2628	0.0394	0.2971	0.4285	0.0353	0.0353	1.2015	0.0221	0.1157	1729G
N5286-3021	206.67270	-51.34514	10.9670	0.0882	0.0180	-0.0228	0.5405	0.0134	-0.0056	1.0781	0.0097	-0.0680	1687G
N5286-3022	206.75072	-51.35933	11.6600	-0.2314	0.0456	-0.3015	0.5102	0.0276	0.0072	1.1262	0.0190	-0.0030	5541G
N5286-3023	206.68832	-51.36242	12.1110	0.0271	0.0305	-0.0163	0.4513	0.0230	-0.0237	1.0054	0.0164	-0.1127	1737G
N5286-3024	206.65457	-51.34297	13.4610	-0.0498	0.0513	-0.0134	0.3564	0.0390	-0.0346	1.0702	0.0251	-0.0148	1537G
N5286-3033	206.64291	-51.42208	12.5850	0.4697	0.0388	0.4543	0.4815	0.0384	0.0360	1.1566	0.0255	0.0501	1369G
N5286-3034	206.65366	-51.39170	14.1630	0.2136	0.0601	0.2914	0.3737	0.0531	0.0263	1.0459	0.0351	-0.0219	1529G
N5286-3035	206.61162	-51.43067	13.4270	-0.3975	0.0786	-0.3631	0.2833	0.0489	-0.1098	1.0653	0.0301	-0.0205	947G
N5286-3037	206.60625	-51.40703	14.0950	-0.3722	0.0762	-0.2984	0.3193	0.0470	-0.0323	1.0287	0.0302	-0.0406	827G
N5286-3039	206.69041	-51.41572	12.7890	-0.0149	0.0483	-0.0182	0.4006	0.0365	-0.0322	1.0765	0.0241	-0.0249	1747G
N5286-3040	206.61467	-51.41781	13.1280	-0.1347	0.0411	-0.1180	0.3533	0.0294	-0.0584	1.0432	0.0192	-0.0499	996G
N5286-3042	206.58870	-51.42358	12.0010	-0.0442	0.0330	-0.0941	0.4462	0.0237	-0.0356	1.2179	0.0148	0.0971	587G
N5286-3043	206.52225	-51.38350	13.6400	-0.1130	0.0706	-0.0661	0.3493	0.0516	-0.0306	1.1905	0.0308	0.1099	29G
N5286-3044	206.57805	-51.39339	13.6610	-0.2677	0.0531	-0.2195	0.3291	0.0352	-0.0495	1.0672	0.0223	-0.0128	437G
N5286-3045	206.51570	-51.37811	13.4250	-0.0339	0.0397	0.0003	0.3704	0.0302	-0.0228	1.0367	0.0200	-0.0491	17G
N5286-3047	206.55225	-51.38778	13.7410	-0.0787	0.0528	-0.0258	0.3818	0.0387	0.0082	1.1475	0.0242	0.0694	169G
N5286-3048	206.50739	-51.35966	13.4060	-0.3709	0.0473	-0.3378	0.3359	0.0290	-0.0586	1.0584	0.0185	-0.0280	7G
N5286-3049	206.56929	-51.40445	13.7600	0.2490	0.0424	0.3030	0.4271	0.0377	0.0547	1.1281	0.0245	0.0505	289G
N5286-3050	206.57391	-51.36686	12.6600	0.1835	0.0351	0.1725	0.4306	0.0297	-0.0102	1.0876	0.0199	-0.0170	379G
N5286-3051	206.58330	-51.38422	13.0020	-0.0815	0.0586	-0.0723	0.3927	0.0426	-0.0269	1.1958	0.0261	0.0995	509G
N5286-3053	206.59665	-51.40594	14.1720	-0.0480	0.0580	0.0304	0.3662	0.0437	0.0193	1.0408	0.0288	-0.0267	707G
N5286-3055	206.55904	-51.34925	14.0610	-0.2148	0.0740	-0.1430	0.3444	0.0504	-0.0093	1.1065	0.0315	0.0363	207G